The Journal of Experimental Biology 214, 3124-3137

doi:10.1242/jeb.057000

RESEARCH ARTICLE

jShaw1, a low-threshold, fast-activating K_v3 from the hydrozoan jellyfish *Polyorchis penicillatus*

Rheanna M. Sand[1], Donna M. Atherton[1], Andrew N. Spencer[2] and Warren J. Gallin[1,*]

[1]Department of Biological Sciences, University of Alberta, Edmonton, Alberta T6G 2E9, Canada and [2]Vancouver Island University, 900 Fifth Street, Nanaimo, British Columbia V9R 5S5, Canada

*Author for correspondence (wgallin@ualberta.ca)

Accepted 21 June 2011

SUMMARY

Voltage-gated potassium (K_v) channels work in concert with other ion channels to determine the frequency and duration of action potentials in excitable cells. Little is known about K_v3 channels from invertebrates, but those that have been characterized generally display slow kinetics. Here, we report the cloning and characterization of jShaw1, the first K_v3 isolated from a cnidarian, the jellyfish *Polyorchis penicillatus*, in comparison with mouse $K_v3.1$ and $K_v3.2$. Using a two-electrode voltage clamp on *Xenopus laevis* oocytes expressing the channels, we compared steady-state and kinetic properties of macroscopic currents. jShaw1 is fast activating, and opens at potentials approximately 40 mV more hyperpolarized than the mouse K_v3 channels. There is an inverse relationship between the number of positive charges on the voltage sensor and the half-activation voltage of the channel, contrary to what would be expected with the simplest model of voltage sensitivity. jShaw1 has kinetic characteristics that are substantially different from the mammalian K_v3 channels, including a much lower sensitivity of early activation rates to incremental voltage changes, and a much faster voltage-dependent transition in the last stages of opening. jShaw1 opening kinetics were affected little by pre-depolarization voltage, in contrast to both mouse channels. Similar to the mouse channels, jShaw1 was half-blocked by 0.7 mmol l^{-1} tetraethyl ammonium and 5 mmol l^{-1} 4-aminopyridine. Comparison of sequence and functional properties of jShaw1 with the mouse and other reported K_v3 channels helps to illuminate the general relationship between amino acid sequence and electrophysiological activity in this channel family.

Key words: comparative analysis, potassium channel gating, electrophysiology.

INTRODUCTION

Voltage-gated potassium channels (K_v) are pore-forming membrane proteins essential to the electrical signaling of excitable cells such as neurons and myocytes (Hille, 2001). A specific complement of various ion channel proteins is required to transmit action potentials, and individual channel characteristics modulate the threshold, amplitude, duration and frequency of action potentials. By selectively allowing positive potassium ions to flow out of the cell, K_v channels can prevent, prolong or hasten an action potential depending on intrinsic channel properties such as voltage sensitivity, conductance and the kinetics of activation, deactivation and inactivation. Ultimately, variation in these properties is explained by variation in the primary sequence of the channel protein; therefore, differences in the K_v sequence are key contributors to the functional variation of excitability, both within and between species.

Structurally, K_v channels have four interlocking subunits, each containing a cytoplasmic N-terminal tetramerization domain (T1), six trans-membrane helices (S1 to S6) connected by loop sequences, and a cytoplasmic C-terminal domain. Some K_v channels also contain an inactivation particle in the N terminus. Functionally, residues from the start of S1 to the end of S4 constitute the voltage-sensing domain. Changes in membrane potential exert a force on positive amino acids in S4, providing the primary electromotive force to open the intracellular gates of S6. The S5, P-loop, S6 region forms the pore domain, which consists of a re-entrant pore loop that acts as a potassium-selective filter supported by the S5 and S6 helices (Long et al., 2007).

In humans, 40 distinct K_v genes have been identified (Harmar et al., 2009), with 17 of these belonging to the K_v1 through K_v4 subfamilies. In *Drosophila melanogaster*, alternative splicing produces at least 16 different K_v subunits from four genes: the *Shaker* (K_v1) gene gives rise to seven mRNAs, *Shab* (K_v2) to four, *Shaw* (K_v3) to three and *Shal* (K_v4) to two (Tweedie et al., 2009). Regardless of the mechanism by which it arises, the diversity of K_v sequences in both flies and humans contributes significantly to the functional complexities of their respective nervous systems.

Shaker-type (K_v1) channels are the most varied and well-characterized K_v subtype. They tend to mediate fast-activating currents and generally manifest hyperpolarized threshold potentials, which makes them suited to set the resting membrane potential and modulate excitability. In contrast, characterized mammalian Shaw-type (K_v3) channels generally open with large depolarizations, with V_{50} (the voltage at which conductance is 50% of maximum) values ranging from –1 to +19 mV (Gutman et al., 2005) and display both inactivating (or A-type) and non-inactivating currents. The latter phenotype appears to be optimal for shortening the inter-spike interval of repetitively firing cells (Rudy and McBain, 2001). Much less is known about K_v3 channels from invertebrates, but those that have been profiled generally display slower kinetics than mammalian K_v3 channels. *Drosophila melanogaster* Shaw, often considered the archetypal K_v3 channel, has an extremely negative threshold voltage

of –70 mV and a 95% rise time of 102 ms at 0 mV (Wei et al., 1990). Two other characterized invertebrate K_v3 channels have slower opening kinetics than *D. melanogaster* Shaw, but open at more positive potentials. *Notoplana atomata* (a platyhelminth) $K_v3.1$ appears to take up to 100 ms to fully activate and has a V_{50} of +9.3 mV (Klassen et al., 2006), whereas *Caenorhabditis elegans* egl-36 channels open over a period of 800 ms and half-activate at +63 mV (Johnstone et al., 1997).

The molecular basis of such disparate phenotypes can be better understood by comparison with Shaw channels from organisms that diverged from other metazoans early in evolutionary history, such as cnidarians. This approach has been successful in understanding other K_v subtypes. Probing cDNA from the hydrozoan jellyfish *Polyorchis penicillatus* by degenerate PCR previously yielded two A-type Shaker transcripts, jShak1 and jShak2 (GenBank accession AAB02603 and AAB02604) (Jegla et al., 1995). The short S3–S4 loop and atypical amide residues in S2 of jShak1 proved useful in elucidating the interaction of S4 with other parts of the voltage-sensing domain during activation (Klassen et al., 2008). Two Shal channels have also been characterized from *P. penicillatus*, jShal-alpha-1 and jShal-gamma-1 (AAB39750 and AAB39749) (Jegla and Salkoff, 1997). jShal-gamma does not form functional homotetramers, but co-assembles with A-type jShal alpha subunits to drastically increase the rate of inactivation (Jegla and Salkoff, 1997).

Here, we report the cloning and characterization of jShaw1, isolated from *P. penicillatus* and the first K_v3 channel reported from outside the Bilateria. Using two-electrode voltage clamp analysis of *Xenopus laevis* oocytes injected with *in vitro* transcribed mRNA, we compared the steady-state and kinetic properties and pharmacological sensitivities of macroscopic jShaw1, mouse $K_v3.1$ and mouse $K_v3.2$ currents. Characterization of jShaw1 will help us to understand the general process of activation and inactivation in the K_v3 subfamily, and the diverse roles fast-activating channels play in evolutionarily distant species.

MATERIALS AND METHODS

jShaw1 cloning

Novel K_v genes were found using degenerate PCR primers, designed to target conserved sequences in the pore (MTTVGYGD) and the S6 helix [GVL (T/V) IAL] to amplify from genomic DNA isolated from gonad tissue of *Polyorchis penicillatus* (Eschscholtz 1829) medusae (Jegla et al., 1995). One of the amplified sequences was the starting point for isolating the cDNA of jShaw1.

Total RNA was isolated from *P. penicillatus* medusae collected at the Bamfield Marine Sciences Center using the RNAeasy Midiprep kit (Qiagen, Mississauga, ON, Canada) or by density gradient centrifugation using cesium trifluoroacetate (Okayama et al., 1987). The majority of the bell, which is rich in mesoglea but has few cells, was dissected away, approximately 2 mm above the marginal ring. The remaining material (~300 mg per organism) was then homogenized in 4 ml of homogenization buffer (Qiagen RLT buffer for the RNAeasy kit, guanidinium thiocyanate solution for the density gradient centrifugation method) and processed according to the published instructions. The purified total RNA was stored at –80°C.

cDNA for *P. penicillatus* was reverse transcribed from total RNA. Oligo-dT primed cDNA synthesis was carried out using a ThermoScriptRT or GeneRacer kit (Invitrogen, Burlington, ON, Canada). cDNA ends were amplified using the 5′ RACE and 3′ RACE methods (Frohman, 1994), with nested primers as implemented in the GeneRacer kit. The resulting PCR products were cloned and sequenced. Sequence data from PCR products were assembled into a consensus sequence using Staden (v.1.7.0) software (Staden et al., 2000). The sequence of jShaw1 has been deposited in GenBank (accession no. GQ249160).

Alignments and phylogenetic analysis

A set of 173 K_v3 channel amino acid sequences was retrieved from the most recent update of the Voltage-Gated Potassium Channel Database (VKCDB) (Gallin and Boutet, 2010; Li and Gallin, 2004) and aligned using MUSCLE (Edgar, 2004). Removal of positions with more than 5% gaps yielded a data matrix of 235 characters. This matrix was used to infer a phylogenetic tree using MrBayes (Huelsenbeck and Ronquist, 2001; Ronquist and Huelsenbeck, 2003), with four independent runs, each consisting of four chains run for 10^7 generations with sampling every 100th generation, and with the temperature parameter set to 0.05. A consensus tree was generated from the four runs with a burn-in of the first 50,001 trees. A more limited phylogenetic analysis of only the 18 cnidarian K_v3 channels was performed with a 215-character data set with the same conditions as above, except the temperature parameter was set to 0.2.

Homology modeling

A homology model of jShaw1 was created using the Swiss-Model website (Arnold et al., 2006). The jShaw1 protein sequence was aligned with the rat $K_v1.2$ protein sequence and the alignment was truncated to include just the core channel structure, missing both the N-terminal and C-terminal cytoplasmic domains, which have low similarity between the two sequences. The alignment was then used to model the jShaw1 structure on the structure recently generated by normal mode refinement of the original $K_v1.2$ crystal structure (Chen et al., 2010). The images were created using PyMol v.1.4 (DeLano, 2002).

Expression plasmid construction

Full-length jShaw1 was amplified from cDNA using a sense primer containing an Xho I restriction site followed by the Kozak consensus sequence and the first 31 nucleotides of the open reading frame (ORF), and an antisense primer with an Spe I cut site and 38 bases of sequence including the natural stop codon. *Mus musculus* $K_v3.1$ (GenBank accession no. BC132439) and $K_v3.2$ (GenBank accession no. BC116290) cDNA clone ORFs (OpenBiosystems, Huntsville, AL, USA) were amplified with sense and antisense primers containing Xho I and Spe I sites, respectively. Amplicons were double digested and ligated into the vector pXT7 (Dominguez et al., 1995). After transformation into XL1-Blue *Escherichia coli*, individual colonies were picked from ampicillin selection plates and inoculated into 5 ml overnight cultures [Terrific Broth (Ausubel et al., 1987) with 100 μg ml^{-1} ampicillin]. Plasmid was purified from overnight cultures using a Wizard Miniprep Kit (Promega, Madison, WI, USA) and the full ORFs were sequenced to confirm that no errors had been introduced by PCR.

For preparation of mRNA from the cloned sequences for microinjection, plasmids were linearized with Xba I, resolved on agarose electrophoresis gels and purified using the QiaQuick Gel Extraction Kit (Qiagen). Capped mRNAs were prepared by *in vitro* transcription of the linearized template using the mMessage mMachine T7 polymerase kit (Ambion, Austin, TX, USA), and stored at –80°C.

Expression in *Xenopus laevis* oocytes

Two-year-old *X. laevis* females were anaesthetized in 0.17% ethyl 3-aminobenzoate methanesulfonate salt (MS-222; Sigma-Aldrich, Oakville, ON, Canada) for 40 min prior to ovarian lobectomy. To

access the ovarian lobes, a small incision was made approximately 1 cm lateral to the ventral midline and 1 cm caudal to the pelvic girdle. Once removed, the lobes were manually pulled into 0.5 cm clumps, rinsed three times and treated with 2 mg ml^{-1} collagenase IA (Sigma-Aldrich) in modified Barth's medium [MBM; in mmol l^{-1}: NaCl 88, KCl 1, $Ca(NO_3)_2$ 0.33, $CaCl_2$ 0.41, $MgSO_4$ 0.82, $NaHCO_3$ 2.4, HEPES 10, sodium pyruvate 2.4; supplemented with 0.1 g l^{-1} penicillin G and 0.05 g l^{-1} gentamicin sulfate; pH 7.5 with Tris base] (Huang et al., 1993) for 2 h at room temperature on a rotating shaker. This was followed by a 20–40 min treatment under identical conditions in a hypertonic phosphate solution (100 mmol l^{-1} K_2PO_4, pH 6.5 with HCl) for defolliculation. Mature stage V–VII oocytes were cultured in MBM at 18°C before and after microinjection. Oocytes were injected with 2 to 23 nl of nuclease-free water containing 1 to 5 ng of mRNA using a Nanoject II injector (Drummond Scientific Company, Broomall, PA, USA). The amount of mRNA was adjusted for each channel to minimize artifacts introduced by high expression [>20 μA (Grigoriev et al., 1999)]. Each analysis in the present study is from three separately prepared batches of oocytes that were all injected with a single mRNA species, so the electrophysiological characteristics that are derived are for homotetramers with no additional accessory subunits. There was no significant variation between batches in any of the properties that were measured.

Two-electrode voltage clamp electrophysiology

Recordings were made 1–2 days post-injection using a GeneClamp 500B amplifier (Molecular Devices, Sunnyvale, CA, USA) connected to a PC (Dell, Austin, TX, USA) running pClamp 9 software (Molecular Devices). Data were acquired through a 1322 A analogue-to-digital converter and analyzed using Clampfit 9.2 (Molecular Devices) and SigmaPlot (Systat Software, Inc., Point Richmond, CA, USA). Data were filtered at 1 kHz through a four-pole Bessel filter and sampled at 10 kHz. Pipettes were pulled from 1.5 mm outside diameter borosilicate filament capillary tubing using a PMP-102 automatic puller (MicroData Instrument, Inc., South Plainfield, NJ, USA) to resistances <1 MΩ. Oocytes were bathed in ND96 (in mmol l^{-1}: NaCl 96, KCl 2, $CaCl_2$ 1.8, $MgCl_2$ 1, HEPES 5) at room temperature during all experiments. Leak subtraction was performed using a P/4 protocol. The sum of current from four subthreshold hyperpolarizing pre-pulses, each of amplitude ¼ of the depolarizing pulse amplitude, was subtracted from each sweep. Chloride currents native to *X. laevis* oocytes (Miledi and Parker, 1984) were blocked with 1 mmol l^{-1} diisothiocyanatostilbene-2,2′-disulfonic acid (DIDS), present in the bath solution during steady-state and kinetic analysis protocols. As DIDS is known to interfere with jShak1 and jShak2 channels (Grigoriev et al., 1997), current–voltage (*I–V*) graphs were compared before and after application of DIDS to look for reductions in current. DIDS had no visible effects on either the *I–V* curves or the kinetic behavior of the channels. To ensure the independence of recordings from each sweep, the duration of depolarization in voltage protocols were limited to 50 ms and at least 20 ms recovery time was provided between sweeps.

Steady-state opening of the channels was measured using an isochronal tail current protocol. Oocytes were held at –90 mV for 10 ms before a series of 50 ms depolarizing pulses from –80 to +80 mV in 2 mV steps, followed by a 50 ms step to –50 mV for outward tails and a 100 ms return to –90 mV. Activation kinetics were analyzed using traces from the isochronal tail current protocol, and also using a protocol which took the cell through incremental pre-depolarizing steps (Δ5 mV, 50 ms) immediately before a 50 ms depolarization to +60 mV. Deactivation kinetics were investigated by depolarizing oocytes to +60 mV for 50 ms, then immediately stepping to a range of tail voltages ranging from –70 to –10 mV in 5 mV steps. For experiments using tetraethyl ammonium (TEA) and 4-aminopyridine (4AP) (Sigma-Aldrich), oocytes were subjected to the isochronal tail current protocol and data from the +60 mV pulse are presented. During 4AP experiments, a 10 ms pre-pulse to 40 mV was included to allow access to the intracellular binding site (Shieh and Kirsch, 1994). TEA and 4AP were dissolved in ND96 and delivered by gravity-fed perfusion through Teflon tubing or manually using a Pasteur pipette.

Data analysis

Steady-state voltage–conductance curves were obtained by fitting isochronal tail currents (I_{tail}, μA) to the sum of two exponential decays:

$$I_{tail} = (A_1 e^{-t/\tau 1} + C_1) + (A_2 e^{-t/\tau 2} + C_2) \ , \quad (1)$$

where A is the maximal current (μA), t is time (ms), τ is the time constant (ms) and C is a y-offset, in each of the two terms. The start of the fitting range was set to ~2 ms after the beginning of the tails. The parameters generated by fitting the remainder of the tails with Eqn 1 were used to calculate the predicted current at the beginning of the fitting range. Because the driving force is constant during each tail step, the current is proportional to conductance (G). G was normalized using:

$$G_{normal} = \frac{G}{G_{max}} = \frac{I_{tail}}{I_{tail,max}} \ , \quad (2)$$

for each experiment. Sigmoid conductance–voltage curves were then fitted with a fourth-order Boltzmann relationship (Hodgkin and Huxley, 1952):

$$G = y_0 + \frac{G_{max}}{\left[1 + e^{\frac{-(V - V_{50})}{b}}\right]^4} \ , \quad (3)$$

where V and the half-activation voltage V_{50} are in mV, and b is the slope factor (mV). Because this function is raised to the fourth power, the values for V_{50} and b represent one subunit only. V_{50} values for tetrameric channels were calculated by solving for V when G/G_{max}=0.5.

The pre-opening, early, rising and late phases of activation were analyzed separately. The pre-opening phase was described by the time to threshold, i.e. the time from the beginning of the depolarizing voltage step to the time when current exceeded three standard deviations of baseline and did not decrease afterward (to avoid the stimulus artifact). Baseline values were found by averaging the last 10 data points during the –90 mV holding potential before the step change. The early phase was represented by the threshold to 10% rise time, and the rising phase by the 10% to 90% rise time. All three parameters were plotted against voltage and fitted with single exponential decay functions:

$$t_{rise} = y_0 + A e^{-bV}, \quad (4)$$

where t_{rise} is the rise time (ms). The late phase of activation, or current occurring after the half-maximal point, was isolated and fitted to either a single (for mouse K_v3.1) or the sum of two exponential equations (for jShaw1 and mouse K_v3.2):

$$I = A(1 - e^{-t/\tau}), \quad (5)$$

$$I = y_0 + A_1(1 - e^{-t/\tau 1}) + A_2(1 - e^{-t/\tau 2}). \quad (6)$$

Activation kinetics were also investigated by a pre-depolarization protocol, described above, and current starting 1 ms after the rise to +60 mV was fitted with Eqn 5. The resulting time constants were plotted against voltage.

Deactivation kinetics were examined using a variable tail step protocol, described above. Because the holding potential for each of the deactivation steps was different, the resulting tail currents are a function of channel conductance and the driving force, $V–V_{rev}$, where V_{rev} is the reversal potential for potassium. To account for the different driving forces at the various tail steps, currents were divided by driving force to find conductance:

$$G = \frac{I}{V - V_{rev}} . \quad (7)$$

We used a value of –80 mV for V_{rev} because in all our recordings the reversal potential for K^+ ions was approximately –80 mV and a 5 mV change in the estimated V_{rev} had little effect on the analysis. Tail conductance was fitted by Eqn 1, excluding the first 1 ms, producing fast and slow time constants that were plotted against voltage. The fraction of total conductance described by the fast and slow time constants was also determined at each tail step.

Concentration–effect curves for TEA and 4AP were calculated from the fraction of current relative to no-drug control (I_{drug}) at the end of a +60 mV pulse, and plotting against concentration. Resulting curves were fitted with a four-parameter logistic function:

$$I_{drug} = y_0 + \frac{I_{max}}{1 + \left(\frac{[D]}{IC_{50}}\right)^b} , \quad (8)$$

where I_{max} is the maximum current (μA), [D] is the concentration of the drug (mol l^{-1}) and IC_{50} is the concentration at which inhibition is 50% of maximal (mol l^{-1}).

RESULTS

jShaw1 sequence analysis

Degenerate PCR performed on genomic *P. penicillatus* DNA produced several amplicons extending from the highly conserved K_v pore into the flanking S6 region. Gene-specific primers designed from one of these sequences were used in 5′ and 3′ RACE to obtain a full-length ORF. The jShaw1 mRNA contains an ORF 1935 bp in length (GenBank accession no. GQ249160), coding for a single K_v peptide of 644 residues (GenBank accession no. ACS91465).

BLASTP search (Camacho et al., 2009) of the NCBI non-redundant protein database demonstrates significant alignments with a number of predicted protein sequences from cnidarian genome sequencing projects. The most similar protein sequences from experimentally validated channel sequences are to Shaw (K_v3) channels from *Aplysia californica* (California sea hare; E-value=7e–89), *Panulirus interruptus* (California spiny lobster; E-value=4e–87) and *D. melanogaster* (E-value=6e–87). Each share close to 40% identical and 60% conserved residues with jShaw1. Identification of this channel as a member of the K_v3 family was confirmed by alignment with profiles of different gene family protein sequences using HMMer (Eddy, 2010) and by a large-scale phylogenetic analysis that included sequences from all of the K_v families (not shown).

A phylogenetic tree was inferred with MrBayes (v.3.1.2) using a set of 173 K_v3 channel sequences (Fig. 1). The jShaw1 channel is robustly included within a monophyletic group of cnidarian K_v3 paralogs, basal to a clade of four paralogs from *Hydra magnipapillata* (another hydrozoan). *Nematostella vectensis* (an anthozoan) does not have paralogs within this group. The fact that there are four *H. magnipapillata* channels forming a clade as a sister group of jShaw1 is not due to duplications in the annotation of the *H. magnipapillata* genome, because each of the proteins is encoded on a distinct genomic sequence.

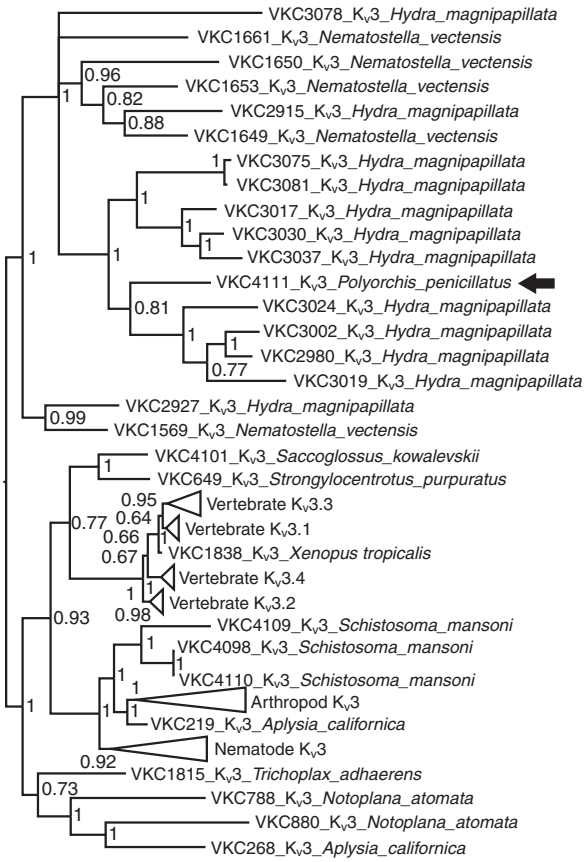

Fig. 1. Phylogenetic tree of the relationships between K_v3 family channel proteins. This tree was inferred using 173 channel sequences. The four vertebrate subfamilies, the arthropod clade and the nematode clade have each been collapsed to a triangle to simplify the presentation. Three cnidarian organisms are included in this tree: the genomes of *Nematostella vectensis*, an anthozoan, and *Hydra magnipapillata*, a hydrozoan, have been sequenced and the channel protein sequences are derived from gene predictions, whereas *Polyorchis penicillatus*, a hydrozoan, is represented by the jShaw1 channel (indicated by a heavy arrow to the right of the tree).

jShaw1 has the typical six trans-membrane domain architecture of K_v channels (Fig. 2A). The N terminus was identified as the first methionine residue after an in-frame stop codon, and the predicted N-terminal sequence aligns well with the N termini of other K_v3 channels.

Multiple alignment of the core jShaw1 peptide sequence (from the N terminus of the first transmembrane helix to the C-terminus of the sixth transmembrane helix) with other K_v3 sequences and *D. melanogaster* Shaker revealed several notable differences (Fig. 2A). jShaw1 has a relatively short S1–S2 linker for a K_v3 channel, 15 residues in length. Most K_v3 channels have S1–S2 loops in the range of 30 to 36 residues: mouse $K_v3.1$ has 34 and mouse $K_v3.2$ has 32. jShaw1 also lacks the N-glycosylation consensus sequence (N-X-S/T) found in the S1–S2 linker of the four other channels of the alignment and in many other K_v sequences. Rat $K_v1.1$, 1.2 and 1.4 are glycosylated at N-X-T sites

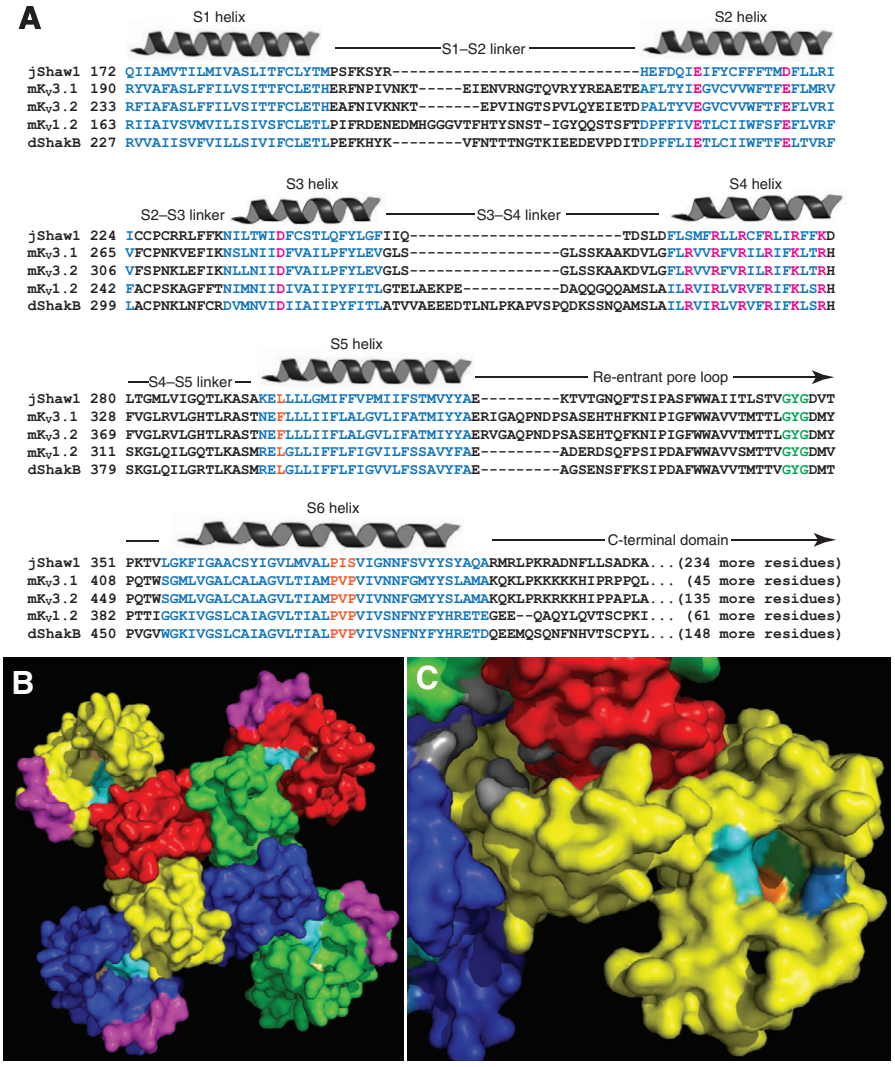

Fig. 2. Structural features of jShaw1. (A) MUSCLE alignment of the jShaw1 protein sequence with mouse $K_v3.1$ and $K_v3.2$, *Drosophila melanogaster* Shaker B, and rat $K_v1.2$. The core structure of the channel, with N-terminal and C-terminal cytoplasmic domains trimmed off, is shown. Numbers indicate the residue number of the first residue shown in each line for each individual channel sequence. Helices are annotated based on alignment to homologous regions in rat $K_v1.2$ and the sequences are indicated in blue. Residues of functional interest are highlighted as follows: S2 and S3 helices – acidic residues (red) that form salt bridges with basic residues in S4; S4 helix – primary voltage-sensing residues (red); S5 region – residue involved in deactivation kinetics (orange); pore loop – potassium selectivity filter (green); S6 helix – conserved PVP hinge site (orange). Channels originated from: jShaw1 – *Polyorchis penicillatus*; dShakB – *Drosophila melanogaster*; mK$_v$3.1 and mK$_v$3.2 – *Mus musculus;* rK$_v$1.2 – *Rattus norvegicus*. (B) Homology model of jShaw1 created using Swiss Model (Arnold et al., 2006), based on a recently refined model of rat $K_v1.2$ (Chen et al., 2010), viewed from the extracellular direction. The subunits in the tetramer are colored red, green, blue and yellow. The S3–S4 loop in each subunit is colored magenta. The basic residues in the S4 helix of each subunit are colored light blue. (C) Same homology model as shown in B, magnified on the yellow subunit and viewed from the cytoplasmic aspect at an angle to give a single view of the residues associated with the voltage sensor. Basic residues in S4 are light blue, F214 is green, D218 is dark blue, D241 is orange, and the PIS motif residues are grey.

(Shi and Trimmer, 1999) and rat $K_v3.1$ is modified at two N-X-T sites in the S1–S2 loop (Cartwright et al., 2007). Jellyfish K_v1 channels jShak1 and jShak2 (Jegla et al., 1995) as well as jShal (a K_v4 channel) contain the N-glycosylation motif in their respective S1–S2 loops.

The S3–S4 loop is also shorter in jShaw1 than in either of the mouse K_v3 channels: eight residues instead of 15. The S4 helix in the K_v3 channels is also apparently shorter than the S4 helix in the K_v1 family of channels, although because this analysis is based on a heuristic homology model it is also possible that the K_v3 S4 helices are as long as the K_v1 S4 helices. In this case, the jShaw1 S3–S4 loop would be even shorter than indicated above.

jShaw1 also differs from the mouse and *D. melanogaster* K_v3 channels in that it has five positively charged residues in the S4 helix – one less than the mouse channels and one more than *D. melanogaster* Shaw. In most voltage-gated channels, the basic residues in S4 can form stabilizing salt-bridges in both the open and closed states with acidic residues in S2 and S3 at positions equivalent to E283, E293 and D316 in *D. melanogaster* Shaker (Decaen et al., 2009; Papazian et al., 1995; Schow et al., 2010; Silverman et al., 2003). jShaw1 shares the same residues aligned with Shaker positions E283 and D316, but has a less bulky aspartate (D218) aligned with Shaker E293 (Fig. 2A). In the cytoplasmic end of S5, jShaw1 differs from the mouse K_v3 channels at a position shown to influence the rate and voltage dependency of deactivation, equivalent to Shaker L396 (Shieh et al., 1997). Here, like both K_v1 channels in the alignment, jShaw1 contains a leucine whereas mouse $K_v3.1$ and $K_v3.2$ contain phenylalanine (Fig. 2A).

The selectivity filter of the jShaw1 pore region is a typical TVGYG sequence. jShaw1 also has a threonine at the position aligned with Shaker T449, a residue linked to TEA sensitivity (MacKinnon and Yellen, 1990). In contrast, the highly conserved PVP hinge sequence in S6 is PIS in jShaw1.

jShaw1 also has a long C terminus, 265 residues, whereas the mouse $K_v3.1$ C-terminal domain is 75 residues, that of $K_v3.2$ is 165 and that of *D. melanogaster* Shaw is 85. jShaw1 lacks an N-terminal inactivation particle as found in the B isoform of the *D. melanogaster* Shaker channel; the total N-terminal sequence prior to the T1 domain is only 18 amino acids in length for jShaw1, whereas the inactivation ball in Shaker B is 20 amino acids long, and is tethered to the end of the T1 domain by a further 41 amino acids. Characterized K_v3 channels do not generally exhibit fast N-type inactivation, with the exception of mammalian $K_v3.4$ (Schroter et al., 1991).

Electrophysiology

Steady-state properties

Microinjection of jShaw1, mouse $K_v3.1$ and mouse $K_v3.2$ mRNA yielded functional channels in *X. laevis* oocytes in as little as 18 h,

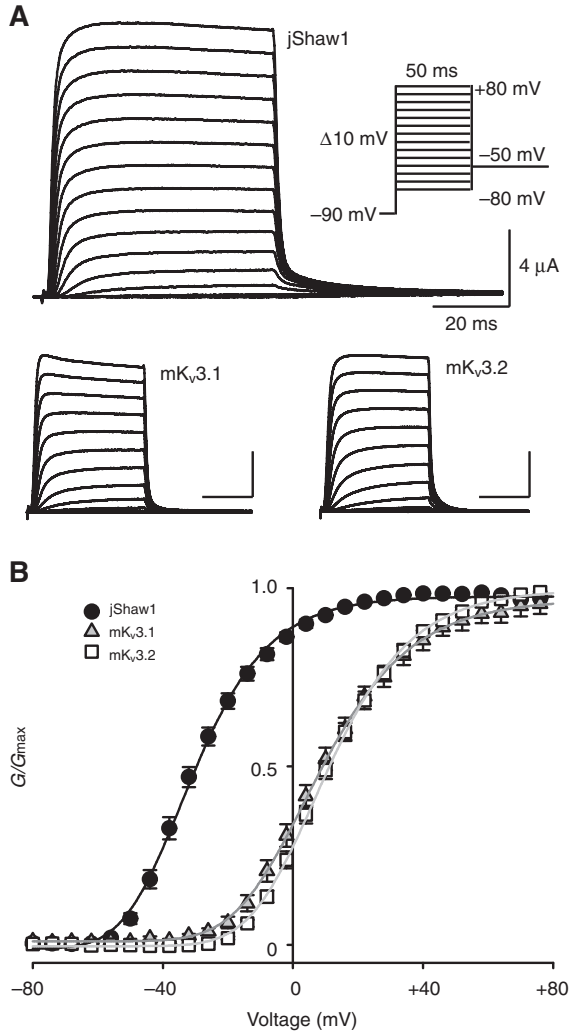

Fig. 3. Steady-state current and conductance of jShaw1, mouse $K_v3.1$ and mouse $K_v3.2$. (A) Representative two-electrode voltage clamp traces from *Xenopus laevis* oocytes expressing the channels. Currents were elicited *via* the depicted voltage protocol. Data are shown in 10 mV increments but were collected in 2 mV steps. Scale bars for $mK_v3.1$ and $mK_v3.2$ have the same values as those shown for jShaw1. (B) Normalized conductance–voltage relationships derived from isochronal tail current analysis for jShaw1 (filled circles), $mK_v3.1$ (shaded triangles) and $mK_v3.2$ (open squares). Solid lines represent the best fit of a Boltzmann function raised to the fourth power. Channel V_{50} values were –29.6 mV for jShaw1, +9.3 mV for $mK_v3.1$ and +11.3 mV for $mK_v3.2$. The differences between the jellyfish *Polyorchis penicillatus* and mouse V_{50} values were both statistically significant (P<0.001), whereas the V_{50} values for the two mouse channels were not different (P=0.376). Boltzmann slopes for single subunits were statistically different between jShaw1 (14.3 mV), $mK_v3.1$ (17.1 mV) and $mK_v3.2$ (15.8 mV), with P-values ranging from <0.001 to 0.014 in pairwise comparisons, although the slopes of the full channels (the fourth order fit) were similar. Data were collected in 2 mV increments but are shown every 4 mV for clarity. Data shown are mean ± s.e.m. (N=9 for each).

as evidenced by robust delayed rectifier currents (Fig. 3A). Some oocytes had maximum currents as high as 40 μA, but to avoid the confounding effects of high channel expression (Grigoriev et al., 1999), we only considered those that yielded a maximum current between 4 and 18 μA. Slight C-type inactivation could be seen during the 50 ms depolarization in all three channels, especially in mouse $K_v3.1$ at higher voltages (Fig. 3A). When stimulated with a series of increasing voltages, jShaw1 channels starting conducting at –45 mV, approximately 25 mV more negative than the threshold of the two mouse channels (Fig. 3B; Table 1) but more positive than –70 mV, the value reported for *D. melanogaster* Shaw (Wei et al., 1990). Isochronal tail current analysis yielded sigmoid conductance–voltage curves that were fitted by a fourth-order Boltzmann relationship, meaning the derived V_{50} and Boltzmann slope values represent that of a single subunit and not the whole channel. Channel V_{50} values were calculated by solving for the voltage that induced conductance equal to half of the maximum (see Materials and methods).

jShaw1 had a single-subunit V_{50} (voltage at which half of the individual subunits in the tetrameric channel were active) of –54.4±6.0 mV and a channel V_{50} (voltage at which half the channel tetramers were open) of –29.6±1.2 mV (N=9; Fig. 3B; Table 1), approximately 40 mV more negative than the mouse channels and significantly different (one-way ANOVA, P<0.001 for both). Mouse $K_v3.1$ had a channel V_{50} of +9.4±1.9 mV (N=9), which was slightly more negative than the published value of +16 mV for this channel in *X. laevis* oocytes (Yokoyama et al., 1989). We found a channel V_{50} of +11.3±1.4 mV (N=9) for mouse $K_v3.2$, and although published V_{50} values for this channel are lacking, our results agree well with those of rat $K_v3.2$, which has a V_{50} of +13 mV (McCormack et al., 1990). Mouse and rat $K_v3.2$ differ by three substitutions and a four-residue insertion in the N-terminal T1 domain and one substitution in the loop between S1 and S2.

The conductance–voltage plot for jShaw1 had a steeper slope in the quasi-linear portion of the curve (Fig. 3B). This was reflected in the Boltzmann slope factor, which indicated that for one jShaw1 subunit, 14.3±0.9 mV were required for an *e*-fold change in conductance (N=9). Mouse $K_v3.1$ and $K_v3.2$ required 17.1 and 15.8 mV per *e*-fold change, respectively (Table 1), and were statistically different from jShaw1 (one-way ANOVA, P=0.012). The mouse channels were not significantly different from each other with respect to V_{50} (P=0.376) but were with respect to single-subunit Boltzmann slope (P=0.014).

Activation kinetics

Activation kinetics were investigated using voltage clamp current traces. The time-to-threshold, early phase rise time (0–10%) and middle phase rise time (10–90%) were evaluated as measures of activation kinetics (Fig. 4D–F). All activation time constants decreased exponentially with increasing voltage and were fit with Eqn 4, a single exponential decay function. To examine how rise times change with voltage, we looked at two parameters from the fit: the *b*-value, or the change in rise time associated with incremental changes in voltage, and the *A*-value, which determines how negatively or positively shifted the response is on the voltage axis.

Threshold times decreased exponentially, approaching an asymptotic value near 1.5 ms for all three channels (Fig. 4D; Table 2). This asymptote could represent either a lower limit to the latency of opening or a limitation of the recording equipment. Single exponential fits produced *b*-values of 0.067, 0.069 and 0.078 for jShaw1, mouse $K_v3.1$ and mouse $K_v3.2$, respectively (Table 2), indicating that mouse $K_v3.2$ was more sensitive to changes in membrane potential than the other two channels. The *A* parameter values for the three channels were 0.047, 0.283 and 0.147, showing that jShaw1 voltage sensitivity was shifted to the most negative potentials, and the $K_v3.2$ channel sensitivity was shifted to a more negative potential than $K_v3.1$.

The time from threshold to 10% of maximum current was also compared across a range of voltages (Fig. 4E). In this phase, the

Table 1. Steady-state properties of *Polyorchis penicillatus* jShaw1 and *Mus musculus* $K_v3.1$ and $K_v3.2$ expressed in *Xenopus laevis* oocytes

Steady-state property	jShaw1	Mouse $K_v3.1$	Mouse $K_v3.2$
Threshold of activation (mV)	–45	–20	–20
Whole-channel V_{50} (mV)	–29.6±1.2 (9)	+9.3±1.9 (9)	+11.3±1.4 (9)
Single-subunit V_{50} (mV)	–54.3±1.7 (9)	–20.0±1.6 (9)	–15.2±1.1 (9)
Single-subunit Boltzman slope (mV e^{-1})	+14.3±0.9 (9)	+17.1±0.5 (9)	+15.8±0.4 (9)

Analyses were performed on whole-cell currents collected by two-electrode voltage clamp. Threshold voltages were approximated from current–voltage graphs (not shown). Whole-channel half-activation voltage (V_{50}) values were derived from the single-subunit V_{50} values as described in the Materials and methods. Data are means ± s.e.m. (*N*), except for threshold voltages.

relationships of rise time to voltage were less steep than those of the pre-opening kinetics. jShaw1 had faster 0–10% times overall, with values ranging from 0.15 to 0.06 ms (Fig. 4E). Mouse $K_v3.2$ was slowest, with values ranging from 0.25 to 0.12 ms. Single exponential decays described the voltage sensitivities well, and produced *b*-values (Table 2) that reveal jShaw1 to be most sensitive to incremental changes in membrane potential. However, the rise times of jShaw1 change the least in the range of voltages tested. This was reflected in the *A* parameter values (Table 2), which show that the absolute sensitivity of jShaw1 is shifted in the negative direction compared with $K_v3.1$, which is shifted more negative than $K_v3.2$.

Mouse $K_v3.1$ manifested the fastest 10–90% rise time: 2.09 ms at +80 mV compared with 4.01 ms for jShaw1 (Fig. 4F). Single exponential fits to the 10–90% rise times against voltage indicate that mouse $K_v3.2$ was least sensitive to incremental changes in voltage. jShaw1 has the lowest absolute sensitivity to voltage

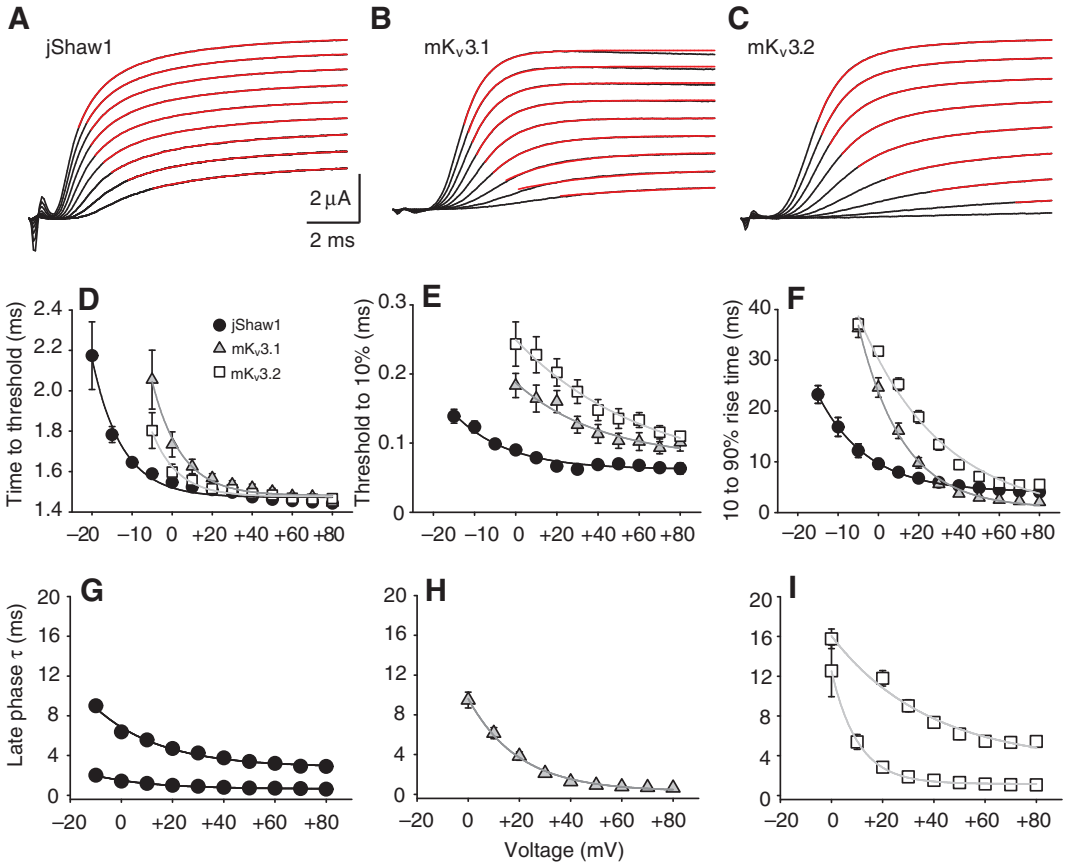

Fig. 4. Activation kinetics of jShaw1, mouse $K_v3.1$ and mouse $K_v3.2$. (A–C) The first 10 ms of voltage clamp currents elicited after stepping to a range of depolarizing voltages from a holding potential of –90 mV. Traces from –10 to +80 mV steps are shown in 10 mV increments. The late phase for each trace, defined as anything above half-maximal, was fitted to a single or a sum of two exponential equations (red lines). The scale bars for jShaw1 apply to all traces. (D) Time to threshold at different activating voltages for jShaw1, $mK_v3.1$ and $mK_v3.2$. Data shown are the time from the beginning of the depolarizing voltage step to the time when current was at least three standard deviations above baseline (see Materials and methods). The voltage sensitivity of time to threshold was fitted with single exponential decays for all three channels (solid lines). (E) Threshold to 10% rise time for jShaw1, $mK_v3.1$ and $mK_v3.2$. The voltage sensitivity of threshold to 10% rise time was fitted with single exponential decays for all three channels (solid lines). (F) 10–90% rise time for jShaw1, $mK_v3.1$ and $mK_v3.2$. The voltage sensitivity of 10–90% rise time was fitted with single exponential decays for all three channels (solid lines). (G–I) Late phase time constants (τ) for jShaw1, $mK_v3.1$ and $mK_v3.2$. τ-values were obtained by averaging the results of the exponential fits described in panels A–C. The voltage sensitivities of late phase τ were fitted with single exponential decays for all three channels (solid lines). For panels D–I, data shown are means ± s.e.m. (*N*=9 for each).

Table 2. Voltage sensitivity of activation and deactivation kinetics for *Polyorchis penicillatus* jShaw1 and *Mus musculus* $K_v3.1$ and $K_v3.2$ expressed in *Xenopus laevis* oocytes

	jShaw1			Mouse $K_v3.1$			Mouse $K_v3.2$		
Kinetic property	*A*	*b*	y_0	*A*	*b*	y_0	*A*	*b*	y_0
Time to threshold	0.047	0.067	1.47	0.283	0.069	1.48	0.147	0.078	1.48
0–10% rise time	0.025	0.039	0.062	0.111	0.024	0.076	0.197	0.016	0.053
10–90% rise time	5.682	0.041	4.03	22.901	0.045	0.83	30.899	0.024	–0.68
Late phase of activation	5.025	0.040	3.52	11.626	0.051	0.39	15.990	0.026	4.06
	1.072	0.045	0.80	–	–	–	14.186	0.097	1.46
Deactivation (conductance)	Invariant	Invariant	Invariant	Invariant	Invariant	Invariant	23.409	0.026	–0.71

Kinetic analyses were performed on whole-cell currents collected by two-electrode voltage clamp. The time to threshold, 0–10% rise time and 10–90% rise time were determined for each channel at a range of depolarizing voltages, and the resulting curves were fitted with single exponential functions (with parameters as shown). The late phase of activation was fitted with a double exponential function and both sets of parameters are shown (except for the late phase of mouse $K_v3.1$ activation, which was fitted with a single exponential). Deactivation kinetics were also described by a double exponential function, with each channel having a voltage-invariant fast term (not shown) and a slow term that was only sensitive to voltage changes in mouse $K_v3.2$. *N*=9 for all activation kinetics; *N*=9 for jShaw1 and mouse $K_v3.1$, and *N*=8 for mouse $K_v3.2$ deactivation kinetics.

because the curve is shifted to the negative (as evidenced by the small *A*-value) but it has an incremental sensitivity to voltage comparable to $K_v3.1$, as indicated by the *b* parameter (0.041 compared with 0.045).

The late phase of activation for all three channels was fitted by exponential functions (Fig. 4A–C, red lines), producing time constants that decreased exponentially with increasing voltage (Fig. 4G–I). Mouse $K_v3.2$ had the longest late phase overall, whereas mouse $K_v3.1$ had the shortest (Fig. 4I). Voltage dependencies of the late phase time constants are listed in Table 2.

Pre-pulse activation kinetics

Delivering pre-pulses of increasing amplitude immediately before a step to +60 mV allowed us to compare the kinetics of the channels

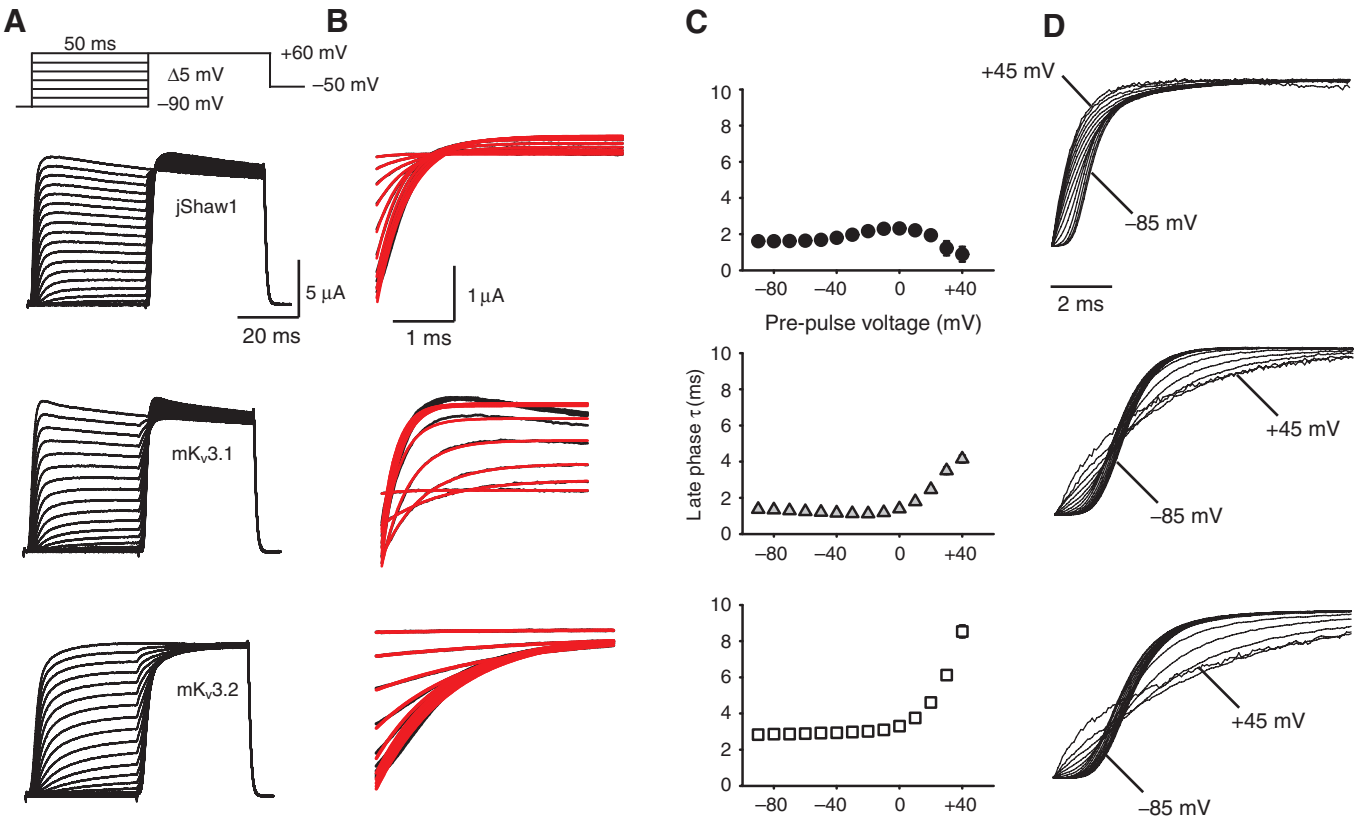

Fig. 5. Kinetics under the influence of pre-activating pulses for jShaw1 compared with mouse $K_v3.1$ and $K_v3.2$. (A) The two-pulse protocol used to investigate the effects of pre-activation voltage on activation kinetics, with representative currents of the three channels expressed in *X. laevis* oocytes. The scale bars shown for jShaw1 apply to both mouse channels. (B) Expanded view of currents shown in A, showing the late phase of activation during the +60 mV pulse (black lines) with single exponential fits (red lines). (C) Time constants (τ) derived from single exponential fits to the late phase of activation for jShaw1 (filled circles; *N*=9), $mK_v3.1$ (grey triangles; *N*=9) and $mK_v3.2$ (open squares; *N*=8) at various pre-depolarizing voltages. τ-values above +40 mV were excluded for clarity. Data shown are means ± s.e.m. (D) Representative full activation traces during the +60 mV pulse scaled and superimposed for jShaw1, $mK_v3.1$ and $mK_v3.2$. Traces collected after pre-depolarizations to –85 and +45 mV are indicated; traces collected above +45 mV were excluded for clarity.

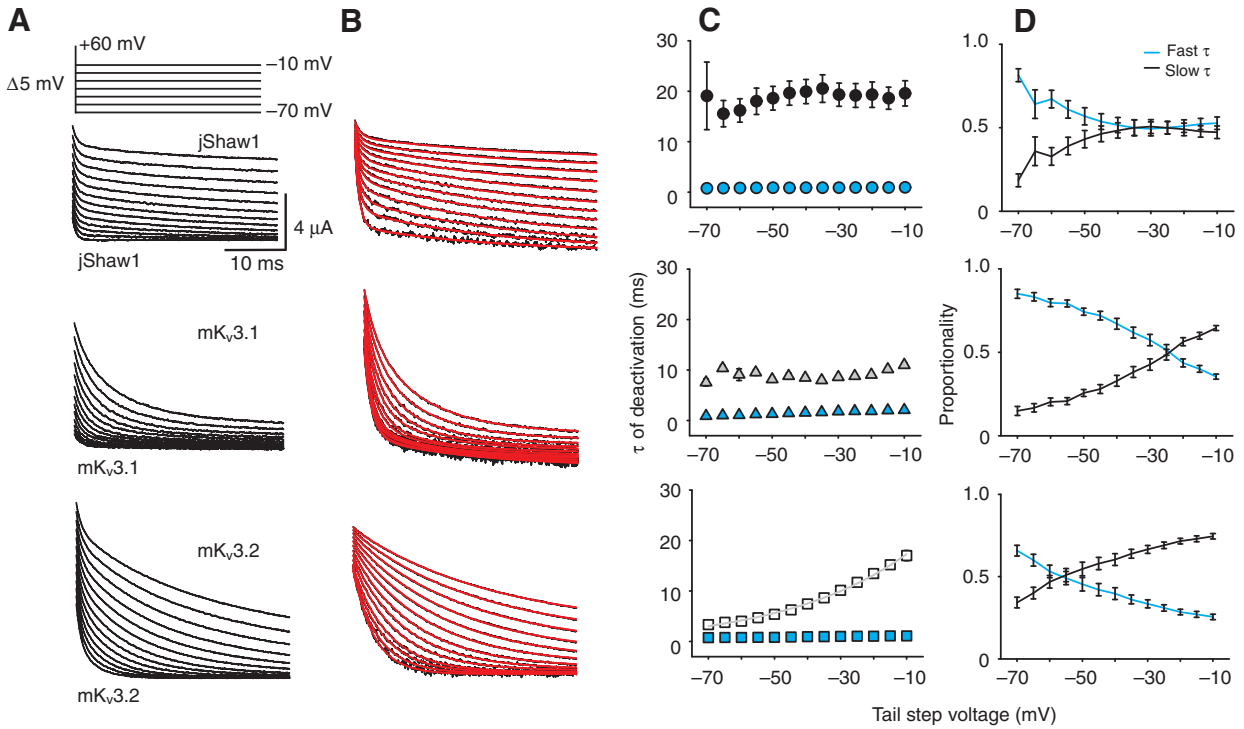

Fig. 6. Deactivation kinetics of jShaw1, mouse K_v3.1 and mouse K_v3.2. (A) Voltage protocol used to elicit tail currents from the three K_v3 channels expressed in *X. laevis* oocytes, with representative traces. Currents shown extend from 0.5 to 35 ms of the 50 ms tail step. Scale bars shown for jShaw1 apply to both mouse channels. (B) Tail conductance, calculated by dividing current by $V–V_{REV}$, with V equal to the tail voltage and an assumed V_{REV} of –80 mV. The time course of conductance was fitted by double exponential decays for all three channels (red lines). (C) Time constants (τ) of deactivation conductance at different tail step voltages for jShaw1 (circles), mK$_v$3.1 (triangles) and mK$_v$3.2 (squares). Fast τ-values appear in cyan. τ-values for all three channels were not fitted with exponential functions, with the exception of the mK$_v$3.2 slow τ (solid grey line). (D) Proportion of conductance described by fast and slow τ-values at different tail voltages. The lines connect data points and do not represent fitted functions. For panels C and D, data shown are means ± s.e.m. (N=9 for jShaw1 and mK$_v$3.1; N=8 for mK$_v$3.2).

as they opened from initial states that occupy different points along their respective activation pathways. The C-type inactivation in jShaw1 and mouse K_v3.1 created a crossover in the current traces as the pre-pulse voltage was increased (Fig. 5A,B). Despite this, activation curves (excluding the first millisecond) were reasonably fitted by single exponential functions for all three channels (Fig. 5B) that yielded time constants with differing degrees of voltage sensitivity (Fig. 5C). The time constant for jShaw1 ranged from 1.5 to a maximum of 2.3 ms; after a small slowing in opening rate with pre-pulses between –40 and +10 mV, the opening kinetics of channels post-pulse became faster as voltage became more positive (Fig. 5C). The opening kinetics of the mouse K_v3 channels, in contrast, conspicuously slowed when the predepolarization exceeded 0 mV. The rescaled traces in Fig. 5D illustrate the difference between the late stages of opening kinetics in jShaw1 and the two mouse channels. Successively more positive depolarizations eliminated the delay phase in the jShaw1 traces, indicating that the later steps in channel activation are rapid, with time constants of less than 2 ms. However, for predepolarization greater than 0 mV in the mouse channels it appears that the residual activation upon depolarization to +60 mV involves a much slower transition, with time constants approaching 10 ms when the predepolarization is +45 mV.

Deactivation kinetics

Deactivation kinetics were examined by maximally opening the channels at +60 mV and then stepping to a series of more negative holding potentials, recording tail currents (Fig. 6A) and converting them to conductance (Fig. 6B) assuming a potassium reversal potential of –80 mV. Tail conductance traces were fitted with the sum of two exponential decays (Fig. 6B, red lines). jShaw1 tail currents decayed more slowly than both mouse channels during the 50 ms tail step, reflected in the slow time constant that was larger than that of either mouse channel, averaging 18.7 ms. Both jShaw1 deactivation time constants were weakly sensitive to voltage, as were those for mouse K_v3.1 (Fig. 6C). This was not the case for mouse K_v3.2; the slow time constant for this channel rose steadily with more positive voltage, rising from 3.3 to 17.0 ms. The proportion of the two deactivation processes described by the two time constants also varied with voltage for all three channels (Fig. 6D). jShaw1 deactivation conductance was dominated by the fast time constant when the tail step was between –70 and –50 mV, but at voltages positive to this, the fast and slow time constants contributed equally. Mouse K_v3.1 and K_v3.2 were each dominated by the fast time constant at the most negative tail step and the slow time constant at the most positive tail step, but the voltage at which the reversal happened was different for the two channels: –25 mV for K_v3.1 and –60 mV for K_v3.2.

Pharmacology

Unlike *D. melanogaster* Shaw (Wei et al., 1990), and similar to the mouse K_v3 channels tested here, jShaw1 was TEA-sensitive (Fig. 7A). jShaw1 currents were half-blocked by 0.7 mmol l^{-1} TEA, which was similar to the 0.3 and 0.7 mmol l^{-1} of mouse K_v3.1 and K_v3.2, respectively (Fig. 7B). For the three channels, Hill coefficients

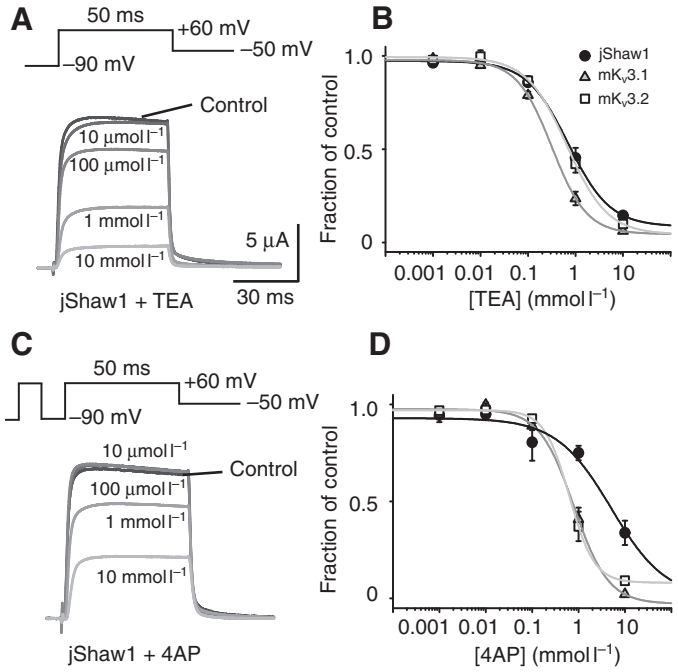

Fig. 7. TEA and 4AP sensitivity of jShaw1 currents. (A) Concentration-dependent TEA blockade of jShaw1 currents elicited by the depicted voltage protocol, recorded from *X. laevis* oocytes expressing the channel. Traces from several cells were normalized to their own control trace and superimposed. (B) Normalized concentration–effect relationship for TEA against jShaw1 compared with both mouse K_v3 channels. Lines represent the best fit of a four-parameter logistic function, and IC_{50} values were 0.7, 0.3 and 0.7 mmol l^{-1} for jShaw1, $mK_v3.1$ and $mK_v3.2$, respectively. (C) Same as A, but with 4AP. In this case, a 10 ms pre-pulse was given to open the channels and allow 4AP to access the intracellular binding site. (D) Same as B, but with 4AP. IC_{50} values were 5.0, 0.8 and 0.6 mmol l^{-1} for jShaw1, $mK_v3.1$ and $mK_v3.2$, respectively. For panels B and D, data shown are means ± s.e.m. Scale bars shown in A apply to all traces.

ranged from 1.0 to 1.2 (Table 3), suggesting a 1:1 stoichiometry of TEA to channel for each of the three channels. jShaw1 was less sensitive to 4AP, as it was only blocked by concentrations above 1 mmol l^{-1} (Fig. 7C). jShaw1 had a higher IC_{50} for 4AP than mouse $K_v3.1$ and $K_v3.2$: ~5 mmol l^{-1} compared with 0.8 and 0.6 mmol l^{-1}, respectively (Fig. 7D). Hill coefficients ranged from 0.7 to 1.2 (Table 3). Our results for the mouse channels compare with previous findings as follows. For mouse $K_v3.1$ we found a TEA IC_{50} of 0.3 mmol l^{-1}, twofold higher than the value of 0.15 mmol l^{-1} previously obtained from oocytes (Grissmer et al., 1992) and 1.5-fold higher than the 0.2 mmol l^{-1} measured from channels expressed in a human cell line (Grissmer et al., 1994), and a 4AP IC_{50} of 0.8 mmol l^{-1}, 1.3-fold to fivefold higher than the published values of 0.6 and 0.18 mmol l^{-1} (Rettig et al., 1992; Yokoyama et al., 1989). For mouse $K_v3.2$, we found a TEA IC_{50} of 0.7 mmol l^{-1} [the reported IC_{50} is ~1 mmol l^{-1} (Lien et al., 2002)], and a 4AP IC_{50} of 0.6 mmol l^{-1} and the published value is ~0.1 mmol l^{-1} (Lien et al., 2002).

DISCUSSION

Phylogenetic analysis clearly groups jShaw1 within the K_v3 family (Fig. 1), but it has distinctions in sequence and function that help illuminate the generalized properties of K_v channels. Functionally, jShaw1 exhibits a mixture of characteristics from other K_v3 channels. The strongly negative activation threshold is reminiscent of *D. melanogaster* Shaw (Wei et al., 1990), but the fast activation is typical of mammalian K_v3 channels (Fig. 3). Strikingly, the V_{50} values for the K_v3 channels are inversely related to the number of charges on the voltage sensor, demonstrating that the simple force generated by the interaction of the membrane potential with the charges on the voltage sensor is not the primary determinant of the overall voltage sensitivity of conductance.

The specific kinetic (Figs 4–6, Table 2) and pharmacological (Fig. 7, Table 3) profiles of jShaw1 also differ between jShaw1, mouse $K_v3.1$ and mouse $K_v3.2$. The characteristic times of the kinetics of jShaw1 respond differently to incremental changes in voltage, compared with the other channels, and are sensitive over a different range of absolute voltage values, indicating that the intramolecular interactions that stabilize the kinetic intermediate conformations are substantially different between the K_v3 channels. Thus, the jShaw1 channel represents novel data on the structure–function relationship in K_v channels.

jShaw1 activation kinetics

The activation of jShaw1 is generally faster than mouse K_v3 channels, but the negative threshold voltage of jShaw1 complicates the interpretation of this result. Looking at Fig. 4D,E, jShaw1 appears to have faster pre-opening and early opening kinetics than the mouse channels, but because jShaw1 has such a negative threshold potential, it is possible that at the –90 mV holding potential there are more jShaw1 channels partitioned into later kinetic intermediate states than is the case for the mouse channels.

jShaw1 and the two mouse channels differ significantly in the late kinetic stages of opening. Comparison of Fig. 4 panels G, H and I shows that the fast component of the late stage of jShak1 activation is faster than that of either mouse K_v3 channel. It is possible to isolate the late-stage kinetics by shifting the channels to intermediate stages of the pre-opening states with a graded set of predepolarization steps (Fig. 5A,B). Predepolarization of jShaw1 acts to decrease the length of latency, indicating that there is a relatively slow step early in the kinetic scheme, but the traces of channel opening after the depolarizations have nearly identical shape when rescaled to a common amplitude (Fig. 5D) and the characteristic time of opening of these late traces shows little change with increasing pre-pulse voltage. In contrast, both of the mouse channels, when predepolarized above 0 mV, not only lack the latency but also show a substantial change in the kinetics of the post-depolarization conductance, with the characteristic rise time increasing to ~10 ms at +45 mV predepolarization pulse. This implies that the mouse K_v3 channels have a very slow kinetic step late in the opening process, whereas jShaw1 shows no sign of such a late slow step.

jShaw1 deactivation kinetics

All three K_v3 channels have deactivation kinetic behavior that is best modeled as the sum of two distinct exponential decays, with a rapid component that is voltage insensitive (Fig. 6C). The slow components of jShaw1 and mouse $K_v3.1$ are also essentially voltage insensitive, so for these two channels, the voltage dependence of deactivation is a product of the relative contribution of the fast and slow processes, not the rates of the processes themselves. Mouse $K_v3.2$, however, has a voltage-sensitive slow component with a characteristic time that increases with increased depolarization, so it displays substantially slower deactivation compared with the other two channels at more positive repolarization potentials (Fig. 6B). In all three channels, the contributions of the fast and slow kinetic components to the overall deactivation process are voltage sensitive

Table 3. Sensitivity of *Polyorchis penicillatus* jShaw1 and *Mus musculus* $K_v3.1$ and $K_v3.2$ to tetraethyl ammonium (TEA) and 4-aminopyridine (4AP)

Pharmacological parameter	jShaw1	Mouse $K_v3.1$	Mouse $K_v3.2$
TEA IC_{50} (mmol l^{-1})	0.7±0.1 (4–6)	0.3±0.0 (5–7)	0.7±0.1 (6)
TEA Hill coefficient	1.0±0.1 (4–6)	1.2±0.1 (5–7)	1.0±0.1 (6)
4AP IC_{50} (mmol l^{-1})	5.0±2.0 (7–15)	0.8±0.1 (6)	0.6±0.0 (4–6)
4AP Hill coefficient	0.7±0.2 (7–15)	1.2±0.3 (6)	1.6±0.0 (4–6)

Analyses were performed on whole-cell currents collected *via* two-electrode voltage clamp of *Xenopus laevis* oocytes expressing the channels. Oocytes were exposed to a single concentration of either TEA or 4AP, and data from several oocytes were averaged at each concentration. Concentration–effect curves were fitted with a logistic function to derive the IC_{50} values (the concentration at which blockage is half-maximal) and Hill coefficients (an estimate of the number of molecules binding per channel). Data are means ± s.e.m. (range of *N*-values used to create the concentration–effect curves).

(Fig. 6D). Generally, the slow component makes a larger contribution to overall deactivation at more positive repolarization potentials. jShaw1 differs from the two mouse channels, in that the slow and fast components plateau at 50% contribution when the repolarization potential is more positive than –45 mV, whereas the slow component in both mouse channels increases continuously. These distinctive differences in the voltage sensitivity of the three different channels can be the basis for a comparative investigation of the mechanisms of channel deactivation.

jShaw1 structure–function relationships

Comparing K_v channel protein sequences and electrophysiological characteristics from basal metazoans, in this case Cnidaria, to the bilateria is a useful approach for identifying regions and residues important for different elements of channel function. The quantitative and qualitative behavior of K_v channels is a complex function of their amino acid sequence and three-dimensional structure. jShaw1 has sequence differences from other channels at several sites that have been proposed to play a role in specific electrophysiological behaviors.

As mentioned above, comparison of the V_{50} values (Fig. 3; Table 1) for jShaw1, mouse $K_v3.1$ and $K_v3.2$ shows that in these channels the more positively charged the residues are in the S4 helix (Fig. 2), the more positive the V_{50}. This counterintuitive finding indicates that the largest factor in setting the V_{50} value for the channels in this family is not the amount of charge on the voltage sensor, but rather the complex of intra-molecular interactions that determine the free energy difference between the open and closed conformations.

Both of the extracellular loops connecting core transmembrane helices (the S1–S2 and S3–S4 loops) are short compared with other K_v channels, particularly the S3–S4 loop. The length of this loop has a significant effect on voltage sensitivity in the K_v1 channels (Gonzalez et al., 2000; Gonzalez et al., 2001; Mathur et al., 1997), HCN channels (Henrikson et al., 2003; Lesso and Li, 2003; Tsang et al., 2004) and L-type Ca^{++} channels (Nakai et al., 1994). It is possible that the shorter loop constrains the relative movement of the C-terminal end of the S3 helix and the N-terminal end of the S4 helix in such a way that energetically favors an open conformation, contributing to the fact that jShaw1 has a more hyperpolarized activation curve that the two mouse K_v3 channels.

Another structural difference between jShaw1 and the mouse K_v3 channels is the presence of aspartate instead of glutamate near the C-terminal end of the S2 helix (Fig. 2A). This residue is at one of three positions that are usually occupied by acidic residues and that form stabilizing salt bridges with the positive voltage-sensing residues of the S4 helix. In the case of jShaw1, the fact that the shorter aspartate side chain is present at this site suggests that in the closed state the distance between the negative charge of the aspartate and positive charges of arginines in S4 will be greater than if the residue were the more typical glutamate. This would lead to less stabilization of the closed state, and thus the observed shift of equilibrium favouring the open state at less depolarizing voltages. This residue is one of those that have recently been reported to form a center for the transfer of gating charge (Tao et al., 2010). The other two residues involved in forming this complex in rat $K_v1.2$ are identical to those present in jShaw1 and form the same kind of seal around the S4 helix near the cytoplasmic surface (Fig. 2C).

The PVP sequence that forms a hinge in the middle of the S6 helix of most K_v channels is replaced by a PIS motif in jShaw1 (Fig. 2A). This motif is responsible for a transition between alpha-helical and 3_{10} helical conformations in this region, which produces a twisting and bending motion that is required for full channel closing during inactivation (Choe and Grabe, 2009). A mutagenesis study on the human $K_v1.1$ channel demonstrated that changing the valine residue in the PVP motif to isoleucine has large effects on both steady-state and kinetic properties of the channel (Imbrici et al., 2009), consistent with differences between the K_v1 and K_v2 family channels, which also differ at this site. The unusual replacement of PVP motif with PIS appears to be unique to the Cnidaria. Of the 180 annotated K_v3 channels in VKCDB, nine have the PIS motif, all from cnidarians.

The slow, voltage-insensitive deactivation of jShaw1 (Fig. 6) might be due in part to a leucine residue in the cytoplasmic end of S5 (Fig. 2). Shieh and colleagues made chimeras of $K_v2.1$ and $K_v3.1$ and found that replacing the leucine equivalent to Shaker position L396 with phenylalanine caused faster, more voltage-dependent deactivation (Shieh et al., 1997). jShaw1, which is slower to deactivate than both mouse channels, contains a leucine at this aligned position compared with phenylalanine in both mouse channels (Fig. 6), supporting a role for this region in modulating deactivation kinetics.

The S4–S5 linker has also been implicated in deactivation kinetics, as it has been shown to interact with S6 residues in an adjacent subunit during the final, concerted channel opening step and the slow first step of deactivation (Batulan et al., 2010). Termed the ‘RELY’ interaction, three residues in the S4–S5 linker (R, E and L in Shaker) interact with a conserved Y in S6 to couple S4 movement to channel opening. In this region, jShaw1 contains a ‘KELY’ interaction, with the arginine replaced by a similarly basic lysine. The two mouse K_v3 channels also lack the arginine but have a neutral asparagine in its place. Because the RELY interaction stabilizes the open state, lacking this interaction may contribute to the faster deactivation kinetics and more positive activation threshold of both mouse K_v3 channels compared with jShaw1.

Our TEA inhibition data are consistent with existing structural models of blockade. MacKinnon and Yellen pointed out Shaker residue T449 as important for external block (MacKinnon and Yellen, 1990). *Drosophila melanogaster* Shaw has an alanine at this position and is insensitive to TEA (Wei et al., 1990). jShaw1 has a threonine here (Fig. 2A), supporting a role for this residue in conferring sensitivity to quaternary ammonium ions. Additionally, mouse $K_v3.1$ and $K_v3.2$ contain a tyrosine at this position, and show a slightly higher TEA sensitivity than jShaw1. This is qualitatively consistent with the finding that a Shaker Y449 mutant was ~50 times more TEA-sensitive than wild-type Shaker (MacKinnon and Yellen, 1990).

Results from the 4AP experiments are consistent with sequence differences between jShaw1 and the mouse $K_v3.2$ channels. The position homologous to Shaker L396 was shown to be important in determining 4AP sensitivity (Shieh and Kirsch, 1994). Leucine was replaced with phenylalanine at this site in $K_v2.1$ and 4AP sensitivity was increased, which aligns with our result that the mouse channels contain phenylalanine and are more 4AP-sensitive than the leucine-containing jShaw1.

jShaw1 in *P. penicillatus*

Polyorchis penicillatus is a small hydrozoan medusa found in the nearshore areas off the entire west coast of North America. Like most jellyfish, it has three core behaviors – swimming, eating and crumpling – which depend on the combined excitability of neurons, myocytes and epithelial cells. The nervous system of *P. penicillatus* has been previously described (Lin et al., 2001; Spencer, 1979; Spencer and Arkett, 1984) and consists of several diffuse nerve nets coordinated by two nerve rings in the bell margin. The nerve rings are functionally divided into the inner motor center with radial projections to swimming motor neurons and an outer integrating center consisting of first- and second-order photosensory cells.

jShaw1 mRNA was isolated from bell margin tissue, but further localization methods (i.e. *in situ* hybridization and immunolocalization) will be needed to identify and quantify the expression in specific cells. However, previous electrophysiological studies (Przysiezniak and Spencer, 1994; Spencer, 1978; Spencer and Arkett, 1984) on *P. penicillatus* indicate cell types that are more likely to express jShaw1 than others, with the caveat that our data were collected from exogenously expressed homomultimeric channels and may differ functionally from native channels, which may form heteromultimers with other subunits or interact with accessory proteins.

Taking those limitations into account, it is clear that two potassium currents isolated from swimming motor neurons of cultured *P. penicillatus* do not match the biophysical characteristics of jShaw1: one was an A-type current, and the other activated slowly (τ=65–250 ms) with a threshold of –30 mV (Przysiezniak and Spencer, 1994). In the outer nerve ring, however, there are two types of neurons that could accommodate a channel like jShaw1. 'Bursting' cells fire regular, spontaneous action potentials that increase to bursts of six when exposed to sudden darkness. Bursting neurons have a resting membrane potential of approximately –40 mV and action potentials lasting approximately 5 ms, so if jShaw1 were expressed here, a fraction of the channels would be open at all times, helping to set the membrane potential but also antagonizing incoming signals and preventing erroneous bursts. The 'oscillating' system never fires action potentials, but displays a ~1 Hz fluctuation of membrane potential (Spencer and Arkett, 1984). A low-threshold channel like jShaw1 could contribute to this fluctuation, as it would be open at voltages where it could influence the resting membrane potential and prevent the cell from depolarizing to the action potential threshold.

Finally, it is possible that jShaw1 is expressed in myocytes. *Polyorchis penicillatus* muscle cells have a resting membrane potential of –70 mV, and during action potentials, the depolarization phase is 46 ms in length, whereas repolarization is twice as fast (Spencer, 1978). The slow action potential upstroke and quick repolarization could be due to a fast non-inactivating potassium current that is active at hyperpolarized potentials – the most prominent features of jShaw1. The epithelial sheets of *P. penicillatus*, however, fire action potentials in the range of 10 ms, and have a resting membrane potential of –55 mV (Spencer, 1978). Given that jShaw1 activates faster than 10 ms, in these cells it would antagonize incoming signals or lengthen the action potential. Thus, it is less likely that jShaw1 is expressed in epithelial sheets.

The clade to which jShaw1 belongs does not include any identified channels from the sea anemone *N. vectensis* (Fig. 1), suggesting that the ancestral gene from which jShaw1 is derived may be specific to the Hydrozoa and absent from the Anthozoa. Looking at the phylogenetic tree in its entirety, it is clear that paralogs in the K_v3 family have evolved independently in the phylum Cnidaria since the divergence from the Bilateria. Moreover, our electrophysiological results demonstrate that different physiological roles for voltage-gated potassium channels have evolved independently in different phyla. In *P. penicillatus*, the delayed rectifiers that activate at strongly negative membrane potentials appear to have evolved in the K_v3 lineage, whereas in the vertebrates the K_v1 family of channels have this property. Conversely, delayed rectifiers with positive thresholds evolved within the K_v1 family of *P. penicillatus* but in the K_v3 family of vertebrates. Further identification and characterization of cnidarian and other invertebrate and vertebrate K_v3 channels will be needed to determine whether this role reversal is unique to *P. penicillatus* or applicable to cnidarians as a whole.

CONCLUSIONS

Of all the mammalian K_v channels, jShaw1 is evolutionarily most closely related to the K_v3 family, but has distinctively different biophysical and pharmacological properties. In mammalian neurons, high-threshold K_v3 channels are optimized to repolarize a cell quickly after an action potential, priming the cell to fire repeatedly (Rudy et al., 1999; Shevchenko et al., 2004). K_v1 channels, in contrast, open at more negative voltages and modulate resting membrane potential and thus excitability in general. The fact that jShaw1 is a fast-activating, low-threshold channel demonstrates clearly that the functional role of K_v channels has not been constrained to ancestral roles during evolution. Rather, in many cases, members from different phylogenetically related families have evolved to have similar functions.

LIST OF SYMBOLS AND ABBREVIATIONS

4AP	4-aminopyridine
b	Boltzmann slope factor
G	conductance
I	current
IC_{50}	concentration at which inhibition is 50% of maximal
K_v	voltage-gated potassium channel
ORF	open reading frame
TEA	tetraethyl ammonium
V	voltage
V_{50}	voltage at which conductance is 50% of maximum
VKCDB	Voltage-Gated Potassium Channel Database
V_{rev}	potassium reversal potential

ACKNOWLEDGEMENTS

We thank the staff of the Bamfield Marine Science Centre, BC, Canada, for collecting *P. penicillatus* individuals and for providing molecular biology facilities on site. Dr Tara L. Klassen assisted in the molecular cloning of jShaw1. This work was supported by a grant from the Canadian Institutes for Health Research to W.J.G. and A.N.S. R.M.S. received student support in the form of an NSERC PGS-D.

REFERENCES

Arnold, K., Bordoli, L., Kopp, J. and Schwede, T. (2006). The SWISS-MODEL workspace: a web-based environment for protein structure homology modelling. *Bioinformatics* **22**, 195-201.

Ausubel, F. M., Brent, R., Kingston, R. E., Moore, D. D., Seidman, J. G., Smith, J. A. and Struhl, K. (1987). *Current Protocols in Molecular Biology*. New York: John Wiley & Sons.

Batulan, Z., Haddad, G. A. and Blunck, R. (2010). An intersubunit interaction between S4–S5 linker and S6 is responsible for the slow off-gating component in Shaker K channels. *J. Biol. Chem.* **285**, 14005-14019.

Camacho, C., Coulouris, G., Avagyan, V., Ma, N., Papadopoulos, J., Bealer, K. and Madden, T. L. (2009). BLAST+: architecture and applications. *BMC Bioinformatics* **10**, 421.

Cartwright, T. A., Corey, M. J. and Schwalbe, R. A. (2007). Complex oligosaccharides are N-linked to Kv3 voltage-gated K^+ channels in rat brain. *Biochim. Biophys. Acta* **1770**, 666-671.

Chen, X., Wang, Q., Ni, F. and Ma, J. (2010). Structure of the full-length Shaker potassium channel Kv1.2 by normal-mode-based X-ray crystallographic refinement. *Proc. Natl. Acad. Sci. USA* **107**, 11352-11357.

Choe, S. and Grabe, M. (2009). Conformational dynamics of the inner pore helix of voltage-gated potassium channels. *J. Chem. Phys.* **130**, 215103.

Decaen, P. G., Yarov-Yarovoy, V., Sharp, E. M., Scheuer, T. and Catterall, W. A. (2009). Sequential formation of ion pairs during activation of a sodium channel voltage sensor. *Proc. Natl. Acad. Sci. USA* **92**, 22498-22503

DeLano, W. L. (2002). *The PyMol User's Manual*. San Carlos, CA: DeLano Scientific.

Dominguez, I., Itoh, K. and Sokol, S. Y. (1995). Role of glycogen synthase kinase 3 beta as a negative regulator of dorsoventral axis formation in *Xenopus* embryos. *Proc. Natl. Acad. Sci. USA* **92**, 8498-8502.

Eddy, S. R. (2010). HMMER: biosequence analysis using profile hidden Markov models. http://hmmer.org/

Edgar, R. C. (2004). MUSCLE: multiple sequence alignment with high accuracy and high throughput. *Nucleic Acids Res.* **32**, 1792-1797.

Frohman, M. A. (1994). On beyond classic RACE (rapid amplification of cDNA ends). *PCR Methods Appl.* **4**, S40-S58.

Gallin, W. J. and Boutet, P. A. (2010). VKCDB: voltage-gated K^+ channel database updated and upgraded. *Nucleic Acids Res.* **39**, D362-D366.

Gonzalez, C., Rosenman, E., Bezanilla, F., Alvarez, O. and Latorre, R. (2000). Modulation of the *Shaker* K^+ channel gating kinetics by the S3–S4 linker. *J. Gen. Physiol.* **115**, 193-208.

Gonzalez, C., Rosenman, E., Bezanilla, F., Alvarez, O. and Latorre, R. (2001). Periodic perturbations in Shaker K^+ channel gating kinetics by deletions in the S3-S4 linker. *Proc. Natl. Acad. Sci. USA* **98**, 9617-9623.

Grigoriev, N. G., Spafford, J. D., Gallin, W. J. and Spencer, A. N. (1997). Voltage sensing in jellyfish *Shaker* K^+ channels. *J. Exp. Biol.* **200**, 2919-2926.

Grigoriev, N. G., Spafford, J. D. and Spencer, A. N. (1999). The effects of level of expression of a jellyfish *Shaker* potassium channel: a positive potassium feedback mechanism. *J. Physiol.* **517.1**, 25-33.

Grissmer, S., Ghanshani, S., Dethlefs, B., McPherson, J. D., Wasmuth, J. J., Gutman, G. A., Cahalan, M. D. and Chandy, K. G. (1992). The Shaw-related potassium channel gene, Kv3.1, on human chromosome 11, encodes the type I K^+ channel in T cells. *J Biol. Chem.* **267**, 20971-20979.

Grissmer, S., Nguyen, A. N., Aiyar, J., Hanson, D. C., Mather, R. J., Gutman, G. A., Karmilowicz, M. J., Auperin, D. D. and Chandy, K. G. (1994). Pharmacological characterization of five cloned voltage-gated K^+ channels, types Kv1.1, 1.2, 1.3, 1.5, and 3.1, stably expressed in mammalian cell lines. *Mol. Pharmacol.* **45**, 1227-1234.

Gutman, G. A., Chandy, K. G., Grissmer, S., Lazdunski, M., McKinnon, D., Pardo, L. A., Robertson, G. A., Rudy, B., Sanguinetti, M. C., Stuhmer, W. et al. (2005). International Union of Pharmacology. LIII. Nomenclature and molecular relationships of voltage-gated potassium channels. *Pharmacol. Rev.* **57**, 473-508.

Harmar, A. J., Hills, R. A., Rosser, E. M., Jones, M., Buneman, O. P., Dunbar, D. R., Greenhill, S. D., Hale, V. A., Sharman, J. L., Bonner, T. I. et al. (2009). IUPHAR-DB: the IUPHAR database of G protein-coupled receptors and ion channels. *Nucleic Acids Res.* **37**, D680-D685.

Henrikson, C. A., Xue, T., Dong, P., Sang, D., Marban, E. and Li, R. A. (2003). Identification of a surface charged residue in the S3–S4 linker of the pacemaker (HCN) channel that influences activation gating. *J. Biol. Chem.* **278**, 13647-13654.

Hille, B. (2001). *Ionic Channels of Excitable Membranes*. Sunderland, MA: Sinauer Associates Inc.

Hodgkin, A. L. and Huxley, A. F. (1952). A quantitative description of membrane current and its application to conduction and excitation in nerve. *J. Physiol.* **117**, 500-544.

Huang, Q. Q., Harvey, C. M., Paterson, A. R., Cass, C. E. and Young, J. D. (1993). Functional expression of Na^+-dependent nucleoside transport systems of rat intestine in isolated oocytes of *Xenopus laevis*. Demonstration that rat jejunum expresses the purine-selective system N1 (*cif*) and a second, novel system N3 having broad specificity for purine and pyrimidine nucleosides. *J. Biol. Chem.* **268**, 20613-20619.

Huelsenbeck, J. P. and Ronquist, F. (2001). MRBAYES: Bayesian inference of phylogenetic trees. *Bioinformatics* **17**, 754-755.

Imbrici, P., Grottesi, A., D'Adamo, M. C., Mannucci, R., Tucker, S. J. and Pessia, M. (2009). Contribution of the central hydrophobic residue in the PXP motif of voltage-dependent K^+ channels to S6 flexibility and gating properties. *Channels* **3**, 39-45.

Jegla, T. and Salkoff, L. (1997). A novel subunit for Shal K^+ channels radically alters activation and inactivation. *J. Neurosci.* **17**, 32-44.

Jegla, T., Grigoriev, N., Gallin, W. J., Salkoff, L. and Spencer, A. N. (1995). Multiple *Shaker* potassium channels in a primitive metazoan. *J. Neurosci.* **15**, 7989-7999.

Johnstone, D. B., Wei, A., Butler, A., Salkoff, L. and Thomas, J. H. (1997). Behavioral defects in *C. elegans egl-36* mutants result from potassium channels shifted in voltage-dependence of activation. *Neuron* **19**, 151-164.

Klassen, T. L., Buckingham, S. D., Atherton, D. M., Dacks, J. B., Gallin, W. J. and Spencer, A. N. (2006). Atypical phenotypes from flatworm Kv3 channels. *J. Neurophysiol.* **95**, 3035-3046.

Klassen, T. L., O'Mara, M. L., Redstone, M., Spencer, A. N. and Gallin, W. J. (2008). Non-linear intramolecular interactions and voltage sensitivity of a kV1 family potassium channel from *Polyorchis penicillatus* (Eschscholtz 1829). *J. Exp. Biol.* **211**, 3442-3453.

Lesso, H. and Li, R. A. (2003). Helical secondary structure of the external S3–S4 linker of pacemaker (HCN) channels revealed by site-dependent perturbations of activation phenotype. *J. Biol. Chem.* **278**, 22290-22297.

Li, B. and Gallin, W. J. (2004). VKCDB: voltage-gated potassium channel database. *BMC Bioinformatics* **5**, 3.

Lien, C. C., Martina, M., Schultz, J. H., Ehmke, H. and Jonas, P. (2002). Gating, modulation and subunit composition of voltage-gated K^+ channels in dendritic inhibitory interneurones of rat hippocampus. *J. Physiol.* **538**, 405-419.

Lin, Y.-C. J., Gallin, W. J. and Spencer, A. N. (2001). The anatomy of the nervous system of the hydrozoan jellyfish, *Polyorchis penicillatus*, as revealed by a monoclonal antibody. *Invert. Neurosci.* **4**, 65-75.

Long, S. B., Tao, X., Campbell, E. B. and Mackinnon, R. (2007). Atomic structure of a voltage-dependent K^+ channel in a lipid membrane-like environment. *Nature* **450**, 376-382.

MacKinnon, R. and Yellen, G. (1990). Mutations affecting TEA blockade and ion permeation in voltage-activated K^+ channels. *Science* **250**, 276-279.

Mathur, R., Zheng, J., Yan, Y. and Sigworth, F. J. (1997). Role of the S3–S4 linker in *Shaker* potassium channel activation. *J. Gen. Physiol.* **109**, 191-199.

McCormack, T., Vega-Saenz de Miera, E. C. and Rudy, B. (1990). Molecular cloning of a member of a third class of Shaker-family K^+ channel genes in mammals. *Proc. Natl. Acad. Sci. USA* **87**, 5227-5231.

Miledi, R. and Parker, I. (1984). Chloride current induced by injection of calcium into *Xenopus* oocytes. *J. Physiol.* **357**, 173-183.

Nakai, J., Adams, B. A., Imoto, K. and Beam, K. G. (1994). Critical roles of the S3 segment and S3–S4 linker of repeat I in activation of L-type calcium channels. *Proc. Natl. Acad. Sci. USA* **91**, 1014-1018.

Okayama, H., Kawaichi, M., Brownstein, M., Lee, F., Yokota, T. and Arai, K. (1987). High efficiency cloning of full-length cDNA; construction and screening of cDNA expression libraries for mammalian cells. *Methods Enzymol.* **154**, 3-28.

Papazian, D. M., Shao, X. M., Seoh, S. A., Mock, A. F., Huang, Y. and Wainstock, D. H. (1995). Electrostatic interactions of S4 voltage sensor in Shaker K^+ channel. *Neuron* **14**, 1293-1301.

Przysiezniak, J. and Spencer, A. N. (1994). Voltage-activated potassium currents in isolated motor neurons from the jellyfish *Polyorchis penicillatus*. *J. Neurophysiol.* **72**, 1010-1019.

Rettig, J., Wunder, F., Stocker, M., Lichtinghagen, R., Mastiaux, F., Beckh, S., Kues, W., Pedarzani, P., Schroter, K. H., Ruppersberg, J. P. et al. (1992). Characterization of a Shaw-related potassium channel family in rat brain. *EMBO J.* **11**, 2473-2486.

Ronquist, F. and Huelsenbeck, J. P. (2003). MrBayes 3: Bayesian phylogenetic inference under mixed models. *Bioinformatics* **19**, 1572-1574.

Rudy, B. and McBain, C. J. (2001). Kv3 channels: voltage-gated K^+ channels designed for high-frequency repetitive firing. *Trends Neurosci.* **24**, 517-526.

Rudy, B., Chow, A., Lau, D., Amarillo, Y., Ozaita, A., Saganich, M., Moreno, H., Nadal, M. S., Hernandez-Pineda, R., Hernandez-Cruz, A. et al. (1999). Contributions of Kv3 channels to neuronal excitability. *Ann. N. Y. Acad. Sci.* **868**, 304-343.

Schow, E. V., Freites, J. A., Gogna, K., White, S. H. and Tobias, D. J. (2010). Down-state model of the voltage-sensing domain of a potassium channel. *Biophys. J.* **98**, 2857-2866.

Schroter, K. H., Ruppersberg, J. P., Wunder, F., Rettig, J., Stocker, M. and Pongs, O. (1991). Cloning and functional expression of a TEA-sensitive A-type potassium channel from rat brain. *FEBS Lett.* **278**, 211-216.

Shevchenko, T., Teruyama, R. and Armstrong, W. E. (2004). High-threshold, Kv3-like potassium currents in magnocellular neurosecretory neurons and their role in spike repolarization. *J. Neurophysiol.* **92**, 3043-3055.

Shi, G. and Trimmer, J. S. (1999). Differential asparagine-linked glycosylation of voltage-gated K^+ channels in mammalian brain and in transfected cells. *J. Membr. Biol.* **168**, 265-273.

Shieh, C. C. and Kirsch, G. E. (1994). Mutational analysis of ion conduction and drug binding sites in the inner mouth of voltage-gated K^+ channels. *Biophys. J.* **67**, 2316-2325.

Shieh, C. C., Klemic, K. G. and Kirsch, G. E. (1997). Role of transmembrane segment S5 on gating of voltage-dependent K^+ channels. *J. Gen. Physiol.* **109**, 767-778.

Silverman, W. R., Roux, B. and Papazian, D. M. (2003). Structural basis of two-stage voltage-dependent activation in K^+ channels. *Proc. Natl. Acad. Sci. USA* **100**, 2935-2940.

Spencer, A. N. (1978). Neurobiology of *Polyorchis*. I. Function of effector systems. *J. Neurobiol.* **9**, 143-157.

Spencer, A. N. (1979). Neurobiology of *Polyorchis*. II. Structure of effector systems. *J. Neurobiol.* **10**, 95-117.

Spencer, A. N. and Arkett, S. A. (1984). Radial symmetry and the organization of central neurones in a hydrozoan jellyfish. *J. Exp. Biol.* **110**, 69-90.

Staden, R., Beal, K. F. and Bonfield, J. K. (2000). The Staden package, 1998. *Methods Mol. Biol.* **132**, 115-130.
Tao, X., Lee, A., Limapichat, W., Dougherty, D. A. and MacKinnon, R. (2010). A gating charge transfer center in voltage sensors. *Science* **328**, 67-73.
Tsang, S. Y., Lesso, H. and Li, R. A. (2004). Critical intra-linker interactions of HCN1-encoded pacemaker channels revealed by interchange of S3–S4 determinants. *Biochem. Biophys. Res. Commun.* **322**, 652-658.
Tweedie, S., Ashburner, M., Falls, K., Leyland, P., McQuilton, P., Marygold, S., Millburn, G., Osumi-Sutherland, D., Schroeder, A., Seal, R. et al. (2009). FlyBase: enhancing *Drosophila* Gene Ontology annotations. *Nucleic Acids Res.* **37**, D555-D559.
Wei, A., Covarrubias, M., Butler, A., Baker, K., Pak, M. and Salkoff, L. (1990). K^+ current diversity is produced by an extended gene family conserved in *Drosophila* and mouse. *Science* **248**, 599-603.
Yokoyama, S., Imoto, K., Kawamura, T., Higashida, H., Iwabe, N., Miyata, T. and Numa, S. (1989). Potassium channels from NG108-15 neuroblastoma-glioma hybrid cells. Primary structure and functional expression from cDNAs. *FEBS Lett.* **259**, 37-42.